22nd International Conference on Ground Control in Mining

New Approach to Evaluate the Stability of Yield Pillars

Khaled Morsy, *Post-Doctoral Fellow*
Syd Peng, *Chairman and C. T. Holland Professor*
West Virginia University
Department of Mining Engineering
Morgantown, WV

Abstract

In this paper a new method to evaluate the stability of yield pillars was introduced. The evaluation of yield pillar stability was conducted in three steps: (1) Estimation of pillar loading – numerical modeling is a good tool to estimate the pillar loading for most of the geological, geometrical and mining conditions. In this study, finite element technique was used to estimate the state of stress, strain, elastic strain energy and plastic energy, etc. at every point within the pillar. (2) Defining the yield pillar loading zones- The proposed method considered the non-uniform stress distribution of yield pillars by dividing the area of the yield pillar into three loading zones, namely core, transition and rib zones. (3) Estimation of stability indicators – an appropriate stability measure was proposed for each loading zone, such as; Core Stability Factor, CSF, Pillar Bump Index, PBI and Rib Instability Index, RIF.

A case study of successful and unsuccessful yield pillar application was used to assess the applicability of the proposed method.

Coal pillar model

Without a good understanding of the stress distribution in a yield pillar, an adequate design of a yield pillar is almost impossible. Wagner [1974] conducted in-situ compression tests for coal pillars in South African coalfield. Figure 1 shows that the stress distribution inside the pillar is not uniform. He illustrated that the pillar failure initiated at the circumference of the pillar and then transferred inwards. It was found that the perimeter of the pillar is capable of carrying relatively little stress but this portion of the pillar provides lateral confinement which enhances the strength of the pillar core.

Using the Drucker-Prager model with mobilized friction angle, Morsy and Peng [2001] showed that the non-uniform stress distribution in the yield pillar can be simulated. Once the yield pillar is developed, three zones of different amount of confinement can be defined (Figure 2), namely core, transition and rib zones. More detailed explanation for those zones is presented below:

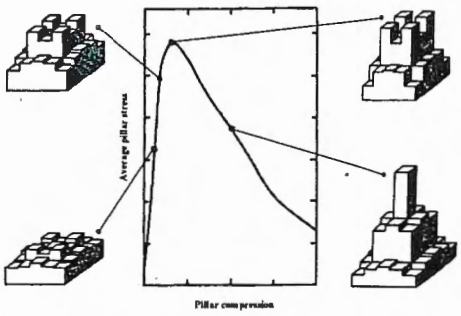

Figure 1 Stress profiles at various stages of pillar compression [after Wagner 1974]

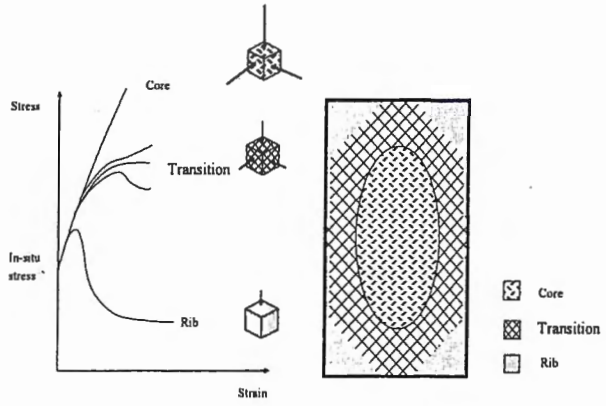

Figure 2 Plane view for yield pillar loading zones

Rib zone – The rib zone occupies the pillar corners (Figure 2). It is the weakest part of the pillar because it is bounded by a free face on two sides, i.e., low confining pressures. The pillar yielding starts from this zone and propagates towards the pillar core. To insure the brittle failure of the rib zone, it is defined as the unstable parts of

the pillar which have post-peak stiffness larger than or equal to the local mining stiffness, Equation 1:

$$|K_p| \geq |K_{LMS}| \quad (1)$$

where $|K_{LMS}|$ is the absolute value of the local mine stiffness; and $|K_p|$ is the absolute value of pillar post-peak stiffness. The numerical methods to estimate the $|K_p|$ and $|K_{LMS}|$ had been published [Morsy and Peng, 2002]

Numerically, the rib zone is capable of carrying relatively little stress but it can not store a large amount of elastic strain energy. Most of the loading energy of the rib zone is dissipated in the form of plastic deformation. The instability of the rib zone can be manifested in the form of coal bounces.

Core zone - The core zone occupies the center portion of the pillar (Figure 2). The core zone is defined as the part of the pillar that does not experience any plastic deformations. The elastic behavior of the core zone is a result of confining stresses applied in this zone. The core zone is capable to withstand extremely high stresses even when the pillar has been compressed beyond its maximum resistance, which is traditionally regarded as the strength of the pillar [Wagner, 1974]. Therefore, the core zone stores a significant amount of elastic strain energy. The more the elastic strain energy retained in the yielded part, the more likely the pillar experiences pillar instability such as coal bumps.

Transition zone – The transition zone is located between the rib and core zones (Figure 2). The transition zone is characterized by a wide range of confining stresses. The transition zone is the most complicated part of the pillar where three types of stress-strain behaviors could be observed for the points located in this zone, namely strain hardening, elastic-plastic and strain-softening with high residual strength. Part of the energy of transition zone is dissipated in the form of plastic deformation while a significant amount of elastic strain energy is stored in this zone. The ratio of elastic strain energy to the dissipated plastic energy governs the stability of the transition zone.

The size of any of the pillar zones depends on many factors, such as the end constraint provided by the roof and floor, pillar width, overburden depth, stage of mining, etc. During different stages of mining, the pillar zones change their sizes and locations. It is not necessary to have all the three loading zones, for example under a condition of relatively low pillar end constraints, the elastic zone could be disappeared.

Yield pillar stability measures

Throughout the following discussion, the yield pillar is assumed to be composed of a number of elements. The stabilities of the pillar zones were evaluated in two steps: first, the stability measure of every element inside the pillar zone is estimated, and second, the stability of the pillar zone is calculated as an average for the stability measures of all the elements located inside the loading zone.

Core stability factor, CSF

The Druker-Prager yield criterion is applied to evaluate the stability of the core zone. The strength criterion evaluates the state of stress in the core with respect to the yield strength. The element stability factor (ESF) is as follows:-

$$ESF = \frac{k + J_1 \tan\alpha}{J_{2D}} \quad (2)$$

where, α and k are the material property constants; J_1 is the first invariant of stress tensor; and J_{2D} is the second invariant of the deviator stress tensor.

Numerically, it is not possible to have ESF less than 1. The possible values for ESF are either 1 for those elements experiencing plastic deformation or greater than 1 for elastic elements. The core stability factor CSF is determined by averaging the element stability factors (ESF) of all elements located within the core zone.

As mentioned earlier, the core zone has the ability to store a significant amount of elastic strain energy. As long as the core stability factor CSF is greater than 1, the elastic strain energy stored in this zone will be in stable condition. This condition is obvious in the stiff pillar design, where the core zone represents most of the pillar and the stress level inside the stiff pillar is less than its yield strength. On other hand the stability of the core is crucial for the yield pillar, especially when the longwall approaches the yield pillar. At that stage of mining, some of the elements inside the core zone start to yield and join the transition zone. Therefore the stored core elastic strain energy could be released to the surrounding in a violence fashion.

Bump Index, BI

Figure 3 shows a typical stress-strain curve for an element located in the transition zone. At any stress level, σ_c, the shaded triangle CED represents the amount of stored strain energy, W_e while the area of polygon OABCE represents the dissipated energy, W_p. In this study, FE technique was used to estimate the state of elastic strain energy and plastic dissipated energy in every element within the pillar. Hence using Equation 2, the element bump index could be calculated as follows [Brauner, 1994]:

$$EBI = \frac{W_e}{W_p} \quad (3)$$

The bump index BI for the transition zone is determined by averaging the element bump indices. The larger the bump index the more elastic energy stored in the pillar and the more tendency for serious coal bumps.

Rib Instability Factor, RIF

The local mine stiffness criterion is used to evaluate the instability of the rib zone. The element instability factor EIF for the rib zone elements is determined by:

$$EIF = \frac{|K_p|}{|K_{LMS}|} \quad (4)$$

Based on the proposed definition of rib zone (Equation 1), the EIF should be greater than 1. The instability factor of the rib zone, RIF is determined by averaging the element instability factors (EIF) of all the elements located in the rib zone. The larger the rib instability factors, the larger the energy that can be released to the surrounding. The RIF covers a wide range of instabilities, from unrecognizable bounces to serious ones.

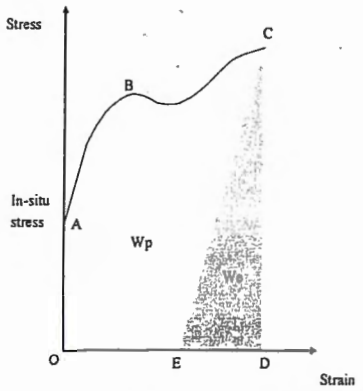

Figure 3 Strain energy storage index, BI for transition zone

Case Study and Method Validation

The U.S. Bureau of Mines (USBM) has long been involved in coal mine bump research as one part of its mission to improve mine safety. As a part of this research, a site monitoring program was carried out in Sunnyside No.1 Mine, UT [Koehler, 1994]. In this paper the USBM monitoring program and its results will be summarized after Koehler [1994, 1996]. The monitoring results will be used to calibrate the three-dimensional FE models for the monitoring sites. A detailed study for these models will be conducted to define the conditions associated with coal bumps. Based on this analysis, a more comprehensive analysis for the proposed method for evaluating yield pillar stability was conducted.

Description of case study

The Sunnyside No. 1 Mine is located in eastern Carbon County, UT. Natural factors conducive to coal bumps at the mines include great depth (as much as 2,950 ft) and massive sandstone strata above and below the coal seam. The field study was located in the two-entry 23rd Left gateroad of the Sunnyside No. 1 mine. The mining height was 7 ft.

The size of pillars at Site 1 was 55-ft x 105-ft and the overburden depth was approximately 2,600 ft. Four BPC's were installed at 9.8, 18, 36.1 and 46 ft measured from the belt entry side in one of the chain pillar. Ten probeholes were drilled in two adjacent pillars at Site 1. Field observations indicated an increase in the frequency and magnitude of rock noise as the longwall approaches Site 1, but no significant coal bump events had been reported. As the mining progressed to a distance of 26-ft inby Site 1, the measurement showed more load was transferred to the pillar core. Coal bumps was reported at a distance of 66 to 100 ft behind the face.

The size of pillars at Site 2 was 40-ft x 105-ft and the overburden depth was approximately 1900 ft. Three BPC's were installed at 10, 20 and 30 ft measured from the belt entry side in one of the chain pillar. Ten probeholes were drilled in two adjacent pillars at Site 2. As the mining progressed to a distance of 213-ft inby Site 2, the recorded pressures in the center of the pillar increased noticeably because of the approach of front abutment pressure. When the face reached Site 2, the monitored pressures suddenly dropped across the pillar width. No coal bumps were known to have occurred in and around Site 2. The data shows that a significant portion of the pillar has yielded nonviolently.

Geology of Sunnyside mine

Generally, five rock types were found in the immediate roof, floor, and interburden between the Lower and Upper beds at the study sites [DeMarco, 1996]: dark-brown mudstone, gray-brown silty sandstone, interbedded siltstone and sandstone, fine-grained quartoze sandstone, and fine-grained calcareous sandstone.

The idealized geological model for the study sites is shown in Figure 4. Each layer of this model is composed of a single homogeneous material. The material parameters used to simulate these layers are given in Table 1.

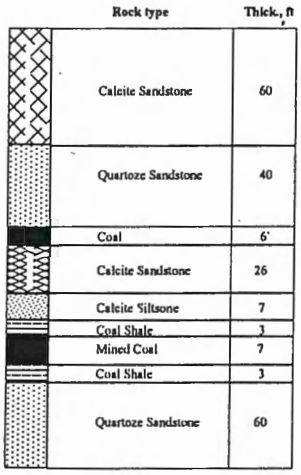

Figure 4 Idealized geological column for Sites 1 and 2

Field simulation

Three-dimensional finite element models were constructed for Sites 1 and 2 (Figure 5). Because the pillar bumps had occurred when the face reached the study site, it was important to calibrate the FE model at that stage of mining. The ABAQUS finite element code [ABAQUS, 1998] was employed to simulate the complex in-situ coal pillar yielding mechanisms. Because of the potentially large model size, two-step modeling technique was employed using the global models and sub-models. 3-D finite global models were created to simulate the geological column shown in Figure 4. At the seam level, the global models considered five blocks of chain pillars, half of the 23rd panel and 100 ft of the 24th panel. The dimensions of the global models were 495 ft x 625 ft x 212 ft and 480 ft x 625 x 212 ft, for Sites 1 and 2, respectively (Figure 5). The

model consisted of 8-node brick elements. Symmetrical conditions were assumed at the middle of the 23rd left Panel. The remaining three side-boundaries and the bottom boundary of the global models were roller-constrained. Simulation of pillar-rock interface was ignored in the global models.

The global model was solved in three steps corresponding to the three different mining stages: geostatic, development, and panel retreat. In the development stage, the gateroads of 20-ft wide were removed. In the panel retreat stage, the 23rd panel face had passed pillar P3 (Figure 5). During the panel retreat, a gob height equivalent to 5 times of mining height was replaced by the gob elements. A detailed description of the gob model employed had been published [Morsy and Peng, 2002]. Perfect elastic-plastic materials were assumed for both rock strata and coal pillars in the global models.

Site 1

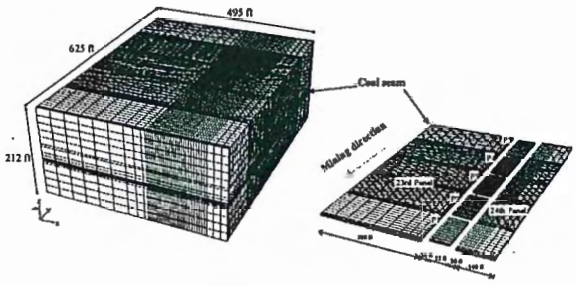

Site 2

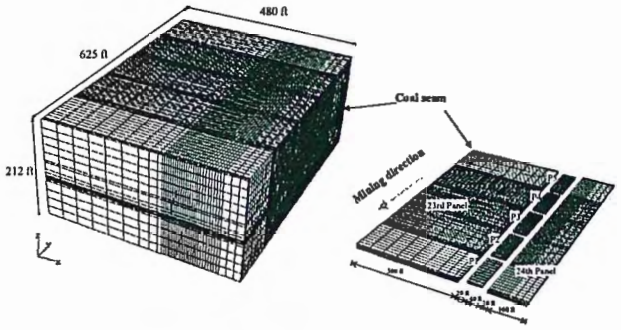

Figure 5 FE global models configurations for Sites 1 and 2

A sub-model for the pillar of interest P3 was solved in three steps as the global model. A strain softening model for coal pillar was considered in the sub-model [Morsy and Peng, 2001]. Perfect elastic-plastic materials were assumed for rock strata. The Coulomb friction model with shear limit was used to simulate the rock/coal interface [ABAQUS manual, 1998]. The interfacial coefficient of friction was assumed to be 0.25. The shear limit of coal/rock interface is the only unknown geotechnical parameter. Because the immediate roof changes significantly throughout the studied gateroad, the shear limit of coal/rock interface should be expected to change accordingly. The collected data at Site 1 shows little pillar yielding. Therefore, high values of coal/rock interface shear limits (325 psi and 500 psi) were tried at Site 1 to match the in-situ measurements with the modeling results. On the other hand, the pillar at Site 2 was completely yielded with the approach of front abutment pressure. Therefore, lower values of coal/rock interface shear limits (150 psi and 325 psi) were tried at Site 2.

Model Calibration

Figure 6 shows the vertical stress distribution across section A-A of the studied pillar at Site 1. It shows the measured pillar pressures at face positions (FP), 0 and 26 ft. A coal/rock interface shear limit of 500 psi shows stress values closer to the in-situ measurements, especially at the belt-entry side of the pillar.

Figure 7 shows the vertical stress distribution across section A-A of the studied pillar at Site 2. For the panel retreat stage, the vertical stress distribution associated with a coal/rock interface shear limit of 325 psi shows high stress values and stress concentration at the belt-entry side of the pillar. These results contradict with the in-situ measurements. On the other hand, the vertical stress distribution associated with a coal/rock interface shear limit of 150 psi shows stress values closer to the in-situ measurements and stress transformation towards pillar center.

From the above discussions, coal/rock interface shear limits of 500 psi and 150 psi were found to be more suitable for Sites 1 and 2, respectively. The difference between the proposed coal/rock interface shear limits at Sites 1 and 2 could be explained by the continuously changes in the immediate roof in the studied gateroad [Maleki, 1995]. The distance between Sites 1 and 2 was 2,310 ft.

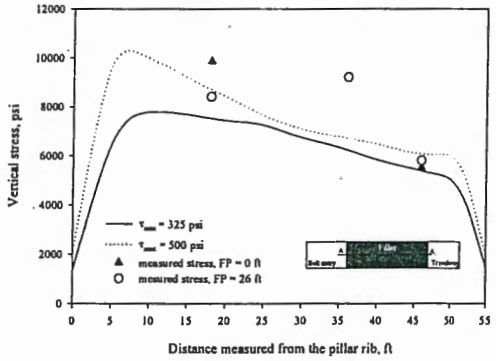

Figure 6 Pillar vertical stress distribution at Site 1

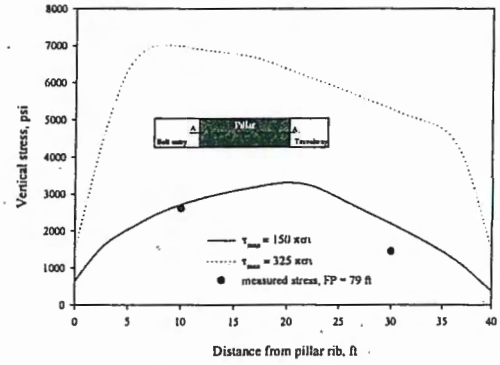

Figure 7 Pillar vertical stress distribution at Site 2

Pillar stability evaluation

The proposed method for evaluating the stability of yield pillars was applied at Sites 1 and 2. Figure 8a shows the loading zones at the mid-section of the pillar at Site 1. The three loading zones, namely, core, transition and rib zones were observed at the development stage. At that stage, the core and transition zones represent a large percentage of the pillar. The rib zone occupies only the pillar corners. Figure 8b shows the zones when the face approached the pillar. It shows that the core zone disappeared completely while the transition and rib zones increased.

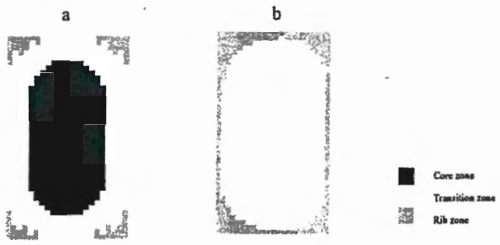

Figure 8 Pillar zones at mid-section for development and panel retreat, Site 1

Figure 9 shows the stress-strain relationships for three elements located in the mid-section of the pillar at Site 1. The solid parts of the stress-strain relationships represent the development stage while the dashed ones represent the panel retreat stage. Element E1 is located at the rib zone while elements E2 and E3 are located in the transition zone. The element E1 shows a strain softening behavior. More than one load deformation pattern are observed in the transition zone. The element E2 shows a strain hardening behavior while element E3 shows a perfect plastic behavior.

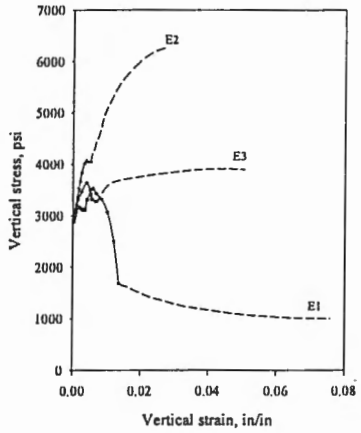

Figure 9 Stress-strain curves at different pillar locations, Site 1

Figure 10 shows the loading zones at the mid-section of the pillar at Site 2. Only two loading zones, namely, transition and rib zones were observed for development and panel retreat stages. There are no significant changes in the sizes of the rib and transition zones during these stages of mining. This could be due to that the pillar had reached its residual strength during the development stage. Therefore no expected changes in the pillar post-peak stiffness during the panel retreat.

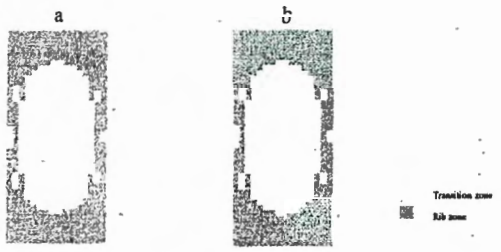

Figure 10 Pillar zones at mid-section for development and panel retreat, Site 2

Figure 11 shows the stress-strain relationships for four elements located in the mid-section of the pillar. The solid parts of the stress-strain relationships represent the development stage while the dashed ones represent the panel retreat stage. Elements E1 is part of the rib zone while elements E2, E3 and E4 are parts of the transition zone. The strain softening behavior of element E1 is the typical pattern for the rib zone. More than one load deformation pattern can be observed in the transition zone. By the end of the development stage, elements E2, E3 and E4 showed strain softening behaviors. During the panel retreat, element E2 continued to maintain the strain softening with high residual strength. The elements E3 and E4 showed strain hardening behaviors.

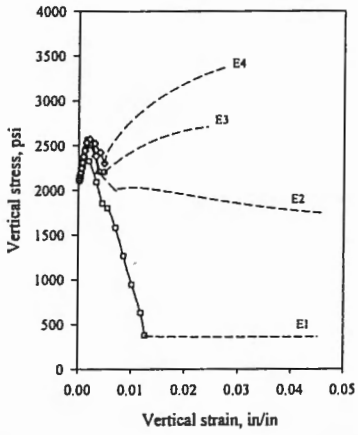

Figure 11 Stress-strain curves at different pillar locations, Site 2

Figure 12 shows the average core stability factors for Sites 1 and 2 at development and panel retreat stages. Site 1 shows small CSF of 1.080 at the development stage but it is still greater than 1. Therefore most of the elements of the elastic core zone were very to their yield strength. Therefore the elastic core zone was considered to be in critical condition where there was a great tendency to release the stored elastic strain energy to the surrounding if more loads are transferred to the elastic core. Site 1

was totally yield during the panel retreat. Site 2 shows a CSF of 1 at the development and panel retreat stages. This means that the elastic core zone was completely destroyed for Site 2 at the development stage.

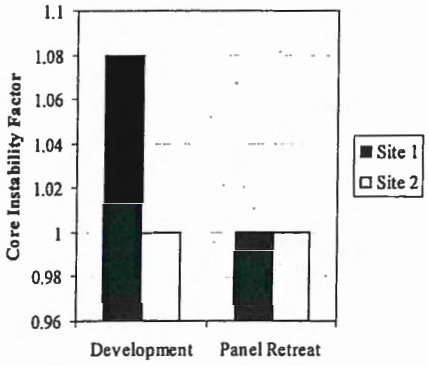

Figure 12 Estimated CSF for pillars at Sites 1 and 2

Figure 13 shows the average bump indices for Sites 1 and 2 at development and panel retreat stages. An average bump index (BI) of 9.570 was estimated for the transition zone of Site 1 after the development stage. The high BI could be one of the reasons for the observed coal bounces activities that observed after the pillar was developed. The analysis showed that the core zone of Site 1 was transferred to transition zone during the panel retreat. Therefore a significant increase in the BI of the transition zone was observed. An average bump index (BI) of 18.89 was estimated for the transition zone when the panel reached Site 1. This high BI could be the main contributor for the coal bump events of Site 1.

Unlike Site 1, Site 2 shows relatively small bump indices at development and panel retreat stages (Figure 13). An average bump index (BI) of 1.711 and 0.533 were estimated for the transition zone of Site 2 at development and panel retreat, respectively. This could be explained by the strain softening behavior of the transition zone during panel retreat in Site 2. On the other hand, the main pattern for the transition zone of Site 1 was strain hardening. This means that the transition zone of Site 2 has a lower tendency for coal bumps and matches with the field observations at Site 2.

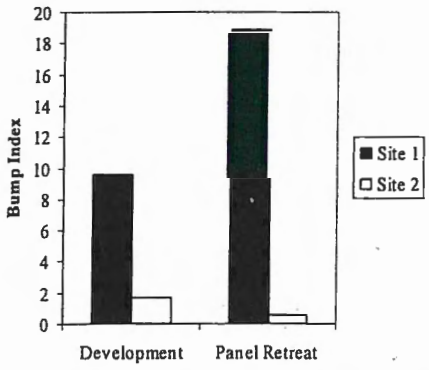

Figure 13 Estimated BI for pillars at Sites 1 and 2

Figure 14 shows the average rib instability factors for Sites 1 and 2 at development and panel retreat stages. An average RIF of 1.76 and 1.83 were estimated for the rib zone of Site 1 at the development and panel retreat stages, respectively. An average RIF of 1.69 and 1.7 were estimated for the rib zone of Site 2 at the development and panel retreat stages. Compared to Site 1, the average RIF for Site 2 was slightly smaller especially at the development stage. This is because of the insignificant difference in K_{LMS} between Sites 1 and 2 since the same immediate roof and floor were presented in both sites.

Comparing the estimated rib instability factors for Sites 1 and 2, similar rib stability at those sites should exist. The field observations in Site 1 explained the noise activities during the development stage as either coal bounces or minor coal bumps. From the above discussion, it is believed that these noise activities were due to coal bumps rather than rib bounces.

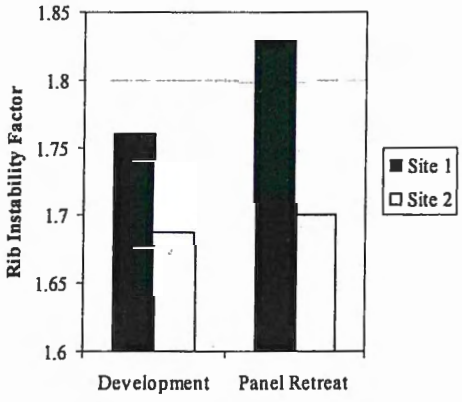

Figure 14 Estimated RIF for pillars at Sites 1 and 2

Conclusions

A new method to evaluate the stability of yield pillars was introduced. The proposed method is designed to evaluate the stability of yield pillar in its post peak loading region. The new method evaluates the yield pillars based on the following assumptions:

- The stresses inside the pillar are not uniformly distributed. Based on the degree of confinement in the pillar, three loading zones, namely; elastic core, transition zone and rib zone could be defined.
- Due to the nouniform stress distribution of coal pillar, more than one stability criterion is required to define the condition for pillar bumps, namely, core stability factor, bump index and rib instability factor.
- The yield pillar instability could be encountered if:
  - The pillar was not able to dissipate its energy in the post peak loading region. Otherwise it stores a significant amount of elastic strain energy.
  - The pillar contains an elastic core during the panel retreat.

Using a case study for successful and unsuccessful yield pillar designs, the proposed method shows the ability to differentiate between both deigns. A significant difference in the estimated bump indices for both designs was obvious.

A detailed study for the effects of geological and geometrical parameters on the proposed method is still required. Also, more study cases are required to define the thresholds of the proposed stability measures.

Acknowledgement

This research was sponsored by CDC (NIOSH) through Grant No. G1R010H04238-01.

References

1. Wagner, H., 1974, "Determination of the Complete Load-Deformation Characteristics of Coal Pillars," Proceedings of the 3rd International Congress on Rock Mechanics, ISRM, Denver, CO, pp. 1076-1081.
2. Morsy, K., and Peng, S., 2001, "Typical Complete Stress-Strain Curves of Coal," Proceedings of the 20th International Conference on Ground Control in Mining. WV U, Morgantown, WV, pp. 210-217.
3. Morsy, K., and Peng, S., 2002, "Evaluation of a mine panel failure using the local mine stiffness criterion-a case study," Transactions of SME, vol. 312, pp. 8 -19.
4. Bräuner. G., 1994, *Rockbursts in Coal Mines and their Prevention*, A. A. Balkema, Rotterdam, Brookfield, 37 p.
5. Koehler, J. R., 1994, "The History of Gateroad Performance at the Sunnyside Mines: Summary of U.S. Bureau of Mines Field Notes," U.S. Bureau of Mines Information Circulation 9393, 43 pp.
6. Koehler, J. R., 1996, "Performance Evaluation 0f a Cable Bolted Yield-Abutment Gateroad System at The Crandall Canyon No.1, Genwall Resources, Inc., Huntington, UT.," 15th International Conference on Ground Control in Mining, CSM, Golden, CO
7. DeMarco, M.J. 1996, "Critical Pillar Concept in Yield-Pillar-Based Longwall Gateroad Design," *Mining Engineering*, August, pp. 73-78.
8. ABAQUS, 1998, *Standard User's Manual*, version 5.8.
9. Morsy, K., and Peng, S. 2002, "Numerical Modeling of the Gob Loading Mechanism in Longwall Coal Mines," Proceedings of the 21st International Conference on Ground Control in Mining. WV U, Morgantown, WV, pp. 58-67.
10. Maleki, H., 1995, "Analysis of Violent Failure in U.S. Coal mines: Case Studies," Proceedings in Mechanics and Mitigation of Violent Failure in Coal and Hard-Rock Mines, USBM special Publication 01-95, pp. 5-25.

Table 1 In-situ material properties for rock mass at Sites 1 and 2

Rock type	Fine-grained calcareous sandstone	Coal	Interbedded siltstone and sandstone	Gray-brown silty sandstone	Dark-brown mudstone	Fine-grained quartoze sandstone
Density lb/ft^3	162	82	162	170	152	154
D-P friction angle, αdeg	61.5	50.9	61.5	50.6	57	46.4
UCS, psi	3,900	1,000	3,900	5,800	1,400	3,600
Poisson's ratio	0.05	0.23	0.05	0.18	0.1	0.07
Young's modulus x10^6, psi	2.06	0.58	2.06	6.15	1.12	1.9

Proceedings
22nd International Conference on Ground Control in Mining

Edited by

Syd S. Peng
Chairman and Charles T. Holland Professor
Department of Mining Engineering
College of Engineering and Mineral Resources
West Virginia University
Morgantown, WV, USA

Christopher Mark
Section Chief, Rock Mechanics
National Institute for Occupational Safety and Health (NIOSH)
Pittsburgh Research Laboratory
Pittsburgh, PA, USA

A. Wahab Khair and Keith Heasley
Professor and Associate Professor
Department of Mining Engineering
College of Engineering and Mineral Resources
West Virginia University
Morgantown, WV, USA

August 5-7, 2003
Lakeview Scanticon Resort & Conference Center, Morgantown, WV, USA

ISBN 0-939084-56-9